

# Nanoscale

## Esterase- and pH-responsive poly( $\beta$ -amino ester)-capped mesoporous silica nanoparticles for drug delivery†

### ELECTRONIC SUPPLEMENTARY INFORMATION

Isurika R. Fernando,<sup>a</sup> Daniel P. Ferris,<sup>a</sup> Marco Frasconi,<sup>a</sup> Dmitry Malin,<sup>b</sup> Elena Strekalova,<sup>b</sup>  
M. Deniz Yilmaz,<sup>a</sup> Michael W. Ambrogio,<sup>c</sup> Mohammed M. Algaradah,<sup>d</sup> Michael P. Hong,<sup>a</sup>  
Xinqi Chen,<sup>c</sup> Majed S. Nassar,<sup>d</sup> Youssry Y. Botros,<sup>d,e</sup> Vincent L. Cryns,<sup>\*b</sup> and J. Fraser Stoddart<sup>\*a</sup>

---

<sup>a</sup>Department of Chemistry, Northwestern University  
2145 Sheridan Road, Evanston, IL 60208, USA  
E-mail: stoddart@northwestern.edu

<sup>b</sup>Department of Medicine, University of Wisconsin Carbone Cancer Center  
University of Wisconsin School of Medicine and Public Health  
3018 WIMR, 1111 Highland Avenue, Madison, WI 53705, USA  
E-mail: vlcryns@medicine.wisc.edu

<sup>c</sup>Northwestern University Atomic and Nanoscale Characterisation and  
Experimental (NUANCE) Center  
Northwestern University, 2220 Campus Drive, Evanston, IL 60208, USA

<sup>d</sup>Joint Center of Excellence in Integrated Nano-Systems (JCIN)  
King Abdul-Aziz City for Science and Technology (KACST)  
P.O. Box 6086, Riyadh 11442, Kingdom of Saudi Arabia

<sup>e</sup>University Research Office, Intel Corporation, Building RNB-6-61  
2200 Mission College Boulevard, Santa Clara, CA 95054, USA

## Table of Contents

### Section

|  |            |
|--|------------|
| <b>1. Materials and General Methods</b>                    | <b>S3</b>  |
| <b>2. Synthesis and Characterisation of Capping Agent</b>  | <b>S4</b>  |
| <b>2.1 Triethylene glycol diacrylate</b>                   | <b>S4</b>  |
| <b>2.2 Poly(<math>\beta</math>-amino ester)</b>            | <b>S5</b>  |
| <b>3. Synthesis of Surface-Modified MSNs</b>               | <b>S7</b>  |
| <b>3.1 Synthesis of AP-MSNs</b>                            | <b>S7</b>  |
| <b>3.2 Synthesis of PBA-MSNs</b>                           | <b>S8</b>  |
| <b>3.3 Synthesis of POL-MSNs</b>                           | <b>S8</b>  |
| <b>4. Characterisation of Functionalised MSNs</b>          | <b>S9</b>  |
| <b>4.1 Powder X-ray diffraction</b>                        | <b>S9</b>  |
| <b>4.2 Nitrogen adsorption-desorption isotherms</b>        | <b>S10</b> |
| <b>4.3 Transmission electron micrographs</b>               | <b>S11</b> |
| <b>4.4 Surface charge</b>                                  | <b>S11</b> |
| <b>4.5 X-Ray photoelectron spectroscopy</b>                | <b>S12</b> |
| <b>4.6 FT-IR spectroscopy</b>                              | <b>S12</b> |
| <b>4.7 Time-of-flight secondary ion mass spectrometry</b>  | <b>S14</b> |
| <b>5. Cargo Loading and Capping</b>                        | <b>S17</b> |
| <b>5.1 Propidium iodide loading and capping</b>            | <b>S17</b> |
| <b>5.2 Doxorubicin loading and capping</b>                 | <b>S17</b> |
| <b>6. Cargo Release Studies in Solution</b>                | <b>S18</b> |
| <b>7. Cargo Uptake and Release Efficiency and Capacity</b> | <b>S19</b> |
| <b>8. Cell Imaging</b>                                     | <b>S20</b> |
| <b>9. In-Vitro Cytotoxicity</b>                            | <b>S21</b> |
| <b>10. References</b>                                      | <b>S21</b> |

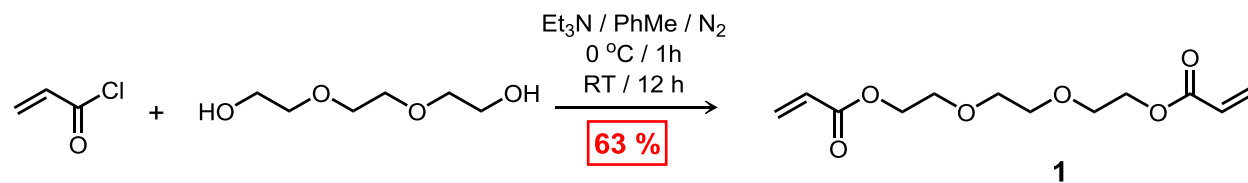
## 1. Materials and General Methods

All reagents were used as received from chemical suppliers (Aldrich and VWR). MCM-41 mesoporous silica nanoparticles (MSNs) were prepared according to a previously reported literature<sup>S1</sup> procedure with minor modifications. Reactions were carried out in anhydrous solvents under an inert nitrogen atmosphere, unless otherwise stated. Thin layer chromatography (TLC) was performed on silica gel 60 F254 TLC plates (Merck) which were viewed under UV light (256 nm and/or 354 nm wavelengths) or developed in an iodine chamber. Column chromatography was carried out on silica gel 60F (Merck 9385, 0.040–0.063 mm). <sup>1</sup>H Nuclear Magnetic Resonance spectra (<sup>1</sup>H NMR) were recorded on a Bruker Avance III instrument operating at 500 MHz at room temperature employing deuterated solvents. High resolution mass spectra (HRMS) were measured on an Agilent 6210 Time of Flight (TOF) LC-MS, employing an electrospray ionization (ESI) source, coupled with an Agilent 1100 HPLC stack using direct infusion (0.6 mL min<sup>-1</sup>). Gel Permeation Chromatography (GPC) was performed using an Agilent 1100 Series isocratic pump, a Rheodine Model 7125 injector and a Phenogel MXL column. Powder X-ray diffraction (XRD) measurements were performed using a Bruker AXS APEX2 diffractometer equipped with a CCD detector and a CuK $\alpha$  I $\mu$ S microfocus source with MX optics. Nitrogen adsorption-desorption measurements were carried out using a Micromeritics, ASAP 2020 Physisorption Analyzer. The transmission electron microscope (TEM) images of the silica were collected on a JEM 1200-EX TEM. Microfilms for TEM imaging were made by placing a drop of a particle suspension in MeOH onto a S3 400-mesh copper TEM grid, followed by drying at room temperature. Zeta ( $\zeta$ ) potentials and particle size distributions of the nanomaterials were measured on a Malvern Instruments, Nano ZS Zetasizer. X-Ray photoelectron spectroscopy (XPS) was performed using a Thermo Scientific ESCALAB

250 Xi. XPS Spectra were calibrated by setting the peak corresponding to the aliphatic carbon at 285 eV. Time-of-flight secondary ion mass spectrometry (ToF-SIMS) was carried out on a Physical Electronics PHI TRIFT III spectrometer. Samples for XPS and ToF SIMS analysis were prepared by affixing double-sided copper tape to a silicon wafer, and subsequently spreading the sample of interest (as a powder) onto the exposed side of the copper tape. FT-IR spectra were recorded on a Thermo Nicolet Nexus 870 spectrometer. pH values were measured with a Mettler Toledo Seven Easy pH-meter. UV-Vis spectra were obtained on a UV-3600 Shimadzu spectrophotometer. Fluorescence spectra were recorded using a Horiba Scientific FluoroMax-4 spectrofluorometer.

## 2. Synthesis and Characterisation of Capping Agent

### 2.1 Triethylene glycol diacrylate



**Scheme S1.** Synthesis of triethylene glycol diacrylate (**1**)

**1:** Acryloyl chloride (4.85 mL, 0.06 mol) was dissolved in PhMe (30 mL) at  $0\text{ }^\circ\text{C}$  and added to a mixture of triethylene glycol (2.67 mL, 0.02 mol) and  $\text{NEt}_3$  (2.60 mL, 0.18 mol) in PhMe (50 mL) at  $0\text{ }^\circ\text{C}$  over 1 h. After complete addition, the solution was slowly warmed up to room temperature and stirred for 12 h. The excess of  $\text{NEt}_3$  was neutralised with 10% HCl solution. The organic phase was washed with  $\text{H}_2\text{O}$  (25 mL x 3) to remove  $\text{NEt}_3$  as its hydrochloride salt, followed by solvent removal by evaporation under reduced pressure. The viscous yellowish-brown, oil-like product was subjected to column chromatography ( $\text{SiO}_2$ : Hexanes : EtOAc, 2:1) the eluent to afford the compound **1** (3.2 g, 63%) as a yellow oil. The sample was stored in dark

at 4 °C until required for polymerisation.  $^1\text{H}$  NMR (500 MHz,  $\text{CD}_3\text{SOCD}_3$ ,  $\delta$ ): 6.45 (dd, 1H,  $\text{CH}_2$ ), 6.20 (m, 1H, CH), 5.86 (dd, 1H,  $\text{CH}_2$ ), 4.26 (t, 2H,  $\text{CH}_2$ ), 3.77 (t, 2H,  $\text{CH}_2$ ), 3.70 (s, 2H,  $\text{CH}_2$ ).

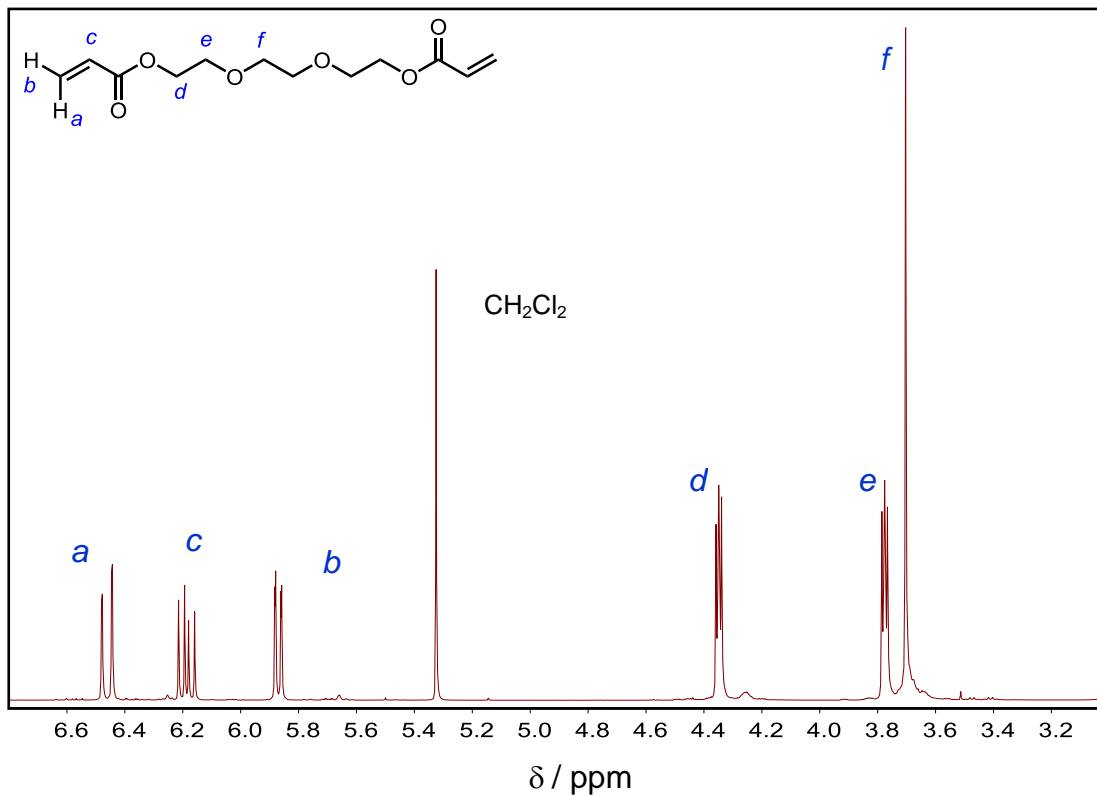
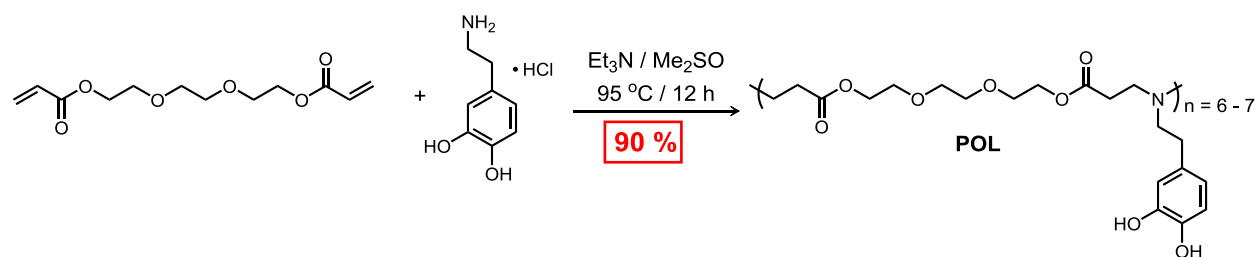


**Fig. S1.**  $^1\text{H}$  NMR Spectrum (500 MHz) of **1** recorded in  $\text{CD}_3\text{COCD}_3$  at 25°C

## 2.2 Poly( $\beta$ -amino ester)

**POL:** Triethylene glycol diacrylate (500 mg, 1.94 mmol), dopamine hydrochloride (367 mg, 1.94 mmol) and  $\text{NEt}_3$  (270  $\mu\text{L}$ , 1.93 mmol) were added to a three-dram vial with a Teflon-lined



**Scheme S2.** Polymerisation of triethylene glycol diacrylate and dopamine hydrochloride via Michael addition reaction

screw cap. Reagents were subsequently dissolved in Me<sub>2</sub>SO (500 μL) and the solution was stirred using a Teflon-coated magnetic stir bar at 95 °C for 12h. Afterwards, Me<sub>2</sub>SO and salts were washed three times with H<sub>2</sub>O by adding H<sub>2</sub>O (2 mL) to precipitate a yellowish colored viscous oily polymer **POL** after decanting the supernant. The purified polymer was characterised by gel permeation chromatography (GPC) and <sup>1</sup>H spectroscopy.

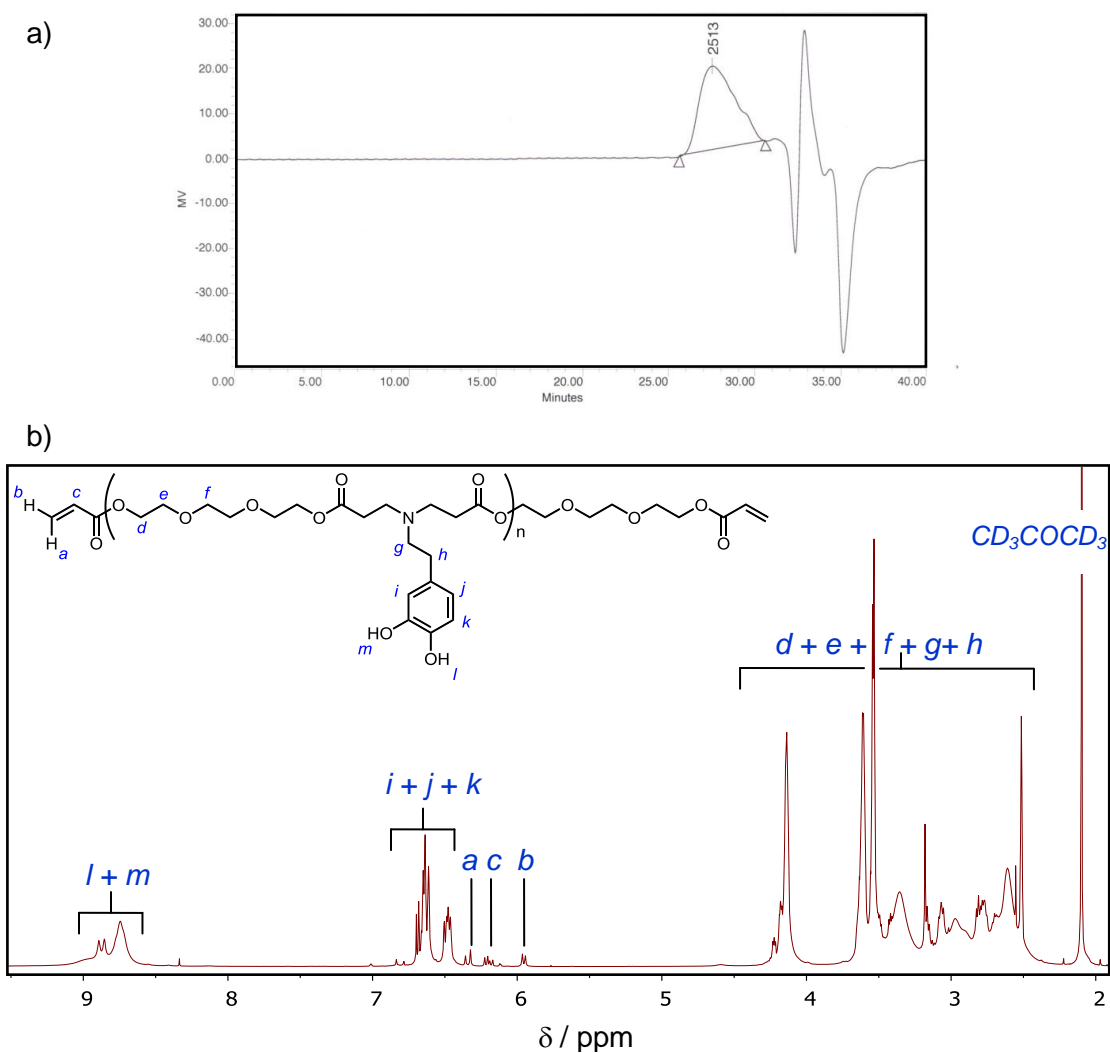


**Fig. S2.** a) Gel permeation chromatograph and b) <sup>1</sup>H NMR spectrum (500 MHz) of **POL** recorded in CD<sub>3</sub>COCD<sub>3</sub> at 25°C

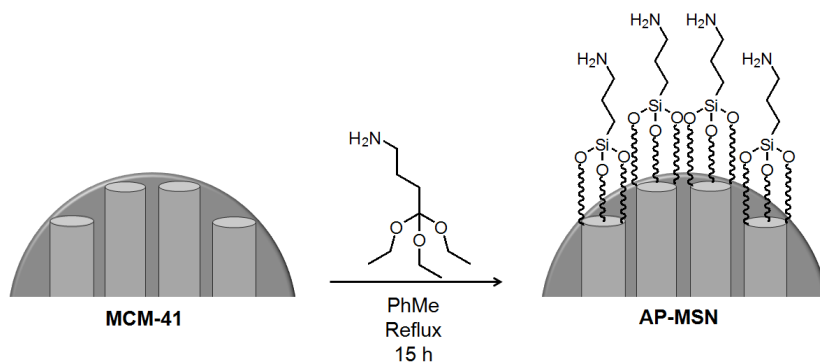
The polymer was stored in dark at 4 °C until use. The GPC chromatogram (Fig. S2a) demonstrated that relative to the monodisperse polystyrene standard, the molecular weight of the

polymer which is 2500, can be attributed to the 6–7 repeating units and the molecular weight distribution is mono-modal with a polydispersity index (PDI) of 1.2. The peaks appear between  $\delta$ : 5.9–6.4 ppm in  $^1\text{H}$  NMR spectra (Fig. S2b) of POL confirms that the end groups of the polymers are acrylate functionalities. This outcome is in an agreement with the literature procedures for poly( $\beta$ -amino ester) synthesis.<sup>S2</sup>

To render the poly( $\beta$ -amino ester) soluble in  $\text{H}_2\text{O}$ , it was dissolved completely in MeOH, diluted with  $\text{Me}_2\text{CO}$  and acidified using HCl. This solution was stirred at room temperature for 1 h. The solvent was then decanted and the polymer was washed with  $\text{Me}_2\text{CO}$  several times.

### 3. Synthesis of Surface Modified MSNs

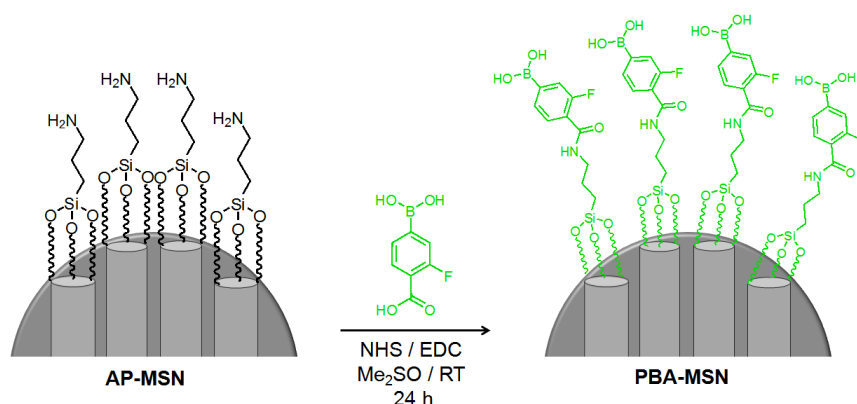
#### 3.1 Amino propyl functionalised MSNs (AP-MSNs)



**Scheme S3.** Synthesis of AP-MSN

Bare MCM-41 particles were suspended in anhydrous PhMe (10 mL) and 3-aminopropyltriethoxysilane (30  $\mu\text{L}$ ) was added slowly with vigorous stirring. After 15 h refluxing, the reaction mixture was cooled to room temperature, concentrated by centrifugation and washed with PhMe, followed by MeOH. For characterisation purposes, a sample of material was dried under vacuum overnight to obtain AP-MSNs. The remaining AP-MSNs particles were solvent exchanged from MeOH to  $\text{Me}_2\text{SO}$  in preparation for PBA modification.

### 3.2 Phenyl boronic acid functionalised MSNs (PBA-MSNs)

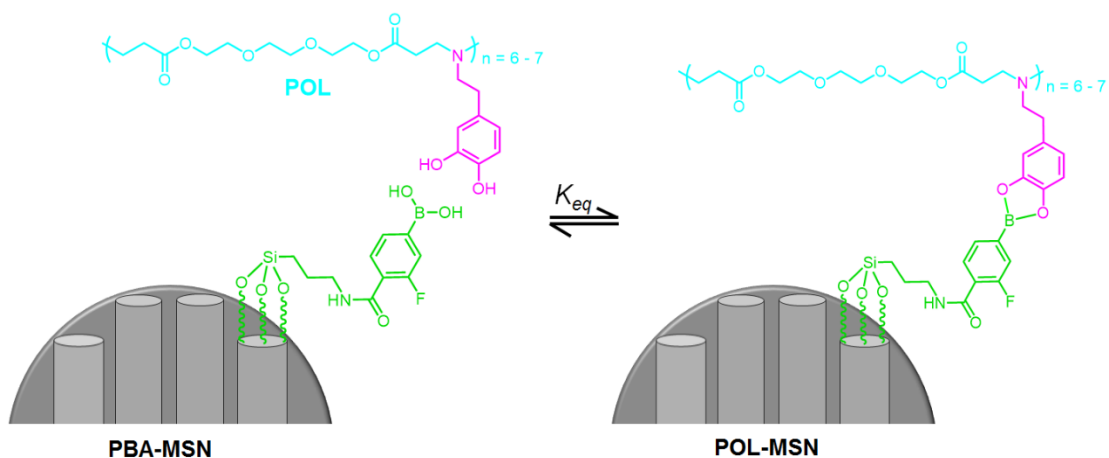


**Scheme S4.** Synthesis of PBA-MSN

4-Carboxy-3-fluorophenylboronic acid (41 mg, 0.225 mmol) was reacted with *N*-hydroxysuccinimide (25 mg, 0.21 mmol) and 1-ethyl-3-(3-dimethylaminopropyl) carbodiimide hydrochloride (50 mg, 0.26 mmol) in Me<sub>2</sub>SO (5 mL) at room temperature for 30 min. This mixture was added to a suspension of AP-MSNs (100 mg) in Me<sub>2</sub>SO (10 mL). After stirring for 24 h at room temperature, the particles were collected by centrifugation and washed with Me<sub>2</sub>SO, followed by MeOH. For characterisation purposes, a fraction of the material was dried under vacuum to obtain PBA-MSNs. The remaining PBA-MSNs particles were solvent-exchanged into aqueous 7.4 PBS buffer solution in preparation for drug loading or polymer capping.

### 3.3 Polymer-capped MSNs (POL-MSNs)

PBA-MSNs (40 mg) were suspended in pH 7.4 PBS buffer (8 mL) and an aqueous solution (1 mL) of the capping agent **POL** (80 mg) was added. The resulting mixture was stirred for another 24 h and POL-MSNs were collected by centrifugation. The POL-MSN product was washed with deionised H<sub>2</sub>O and dried under vacuum to obtain POL-MSNs (36 mg).



**Scheme S5.** Synthesis of POL-MSN

#### 4. Characterisation of Functionalised MSNs

The mesoporous structure and the surface properties of the MCM-41 and the functionalised MSN were characterised using following techniques.

##### 4.1 Powder X-ray diffraction

In order to characterise the mesoporosity of the MSN and evaluate the effect of surface modification on the porosity, powder X-ray diffraction (PXRD) patterns of AP-MSNs, PBA-

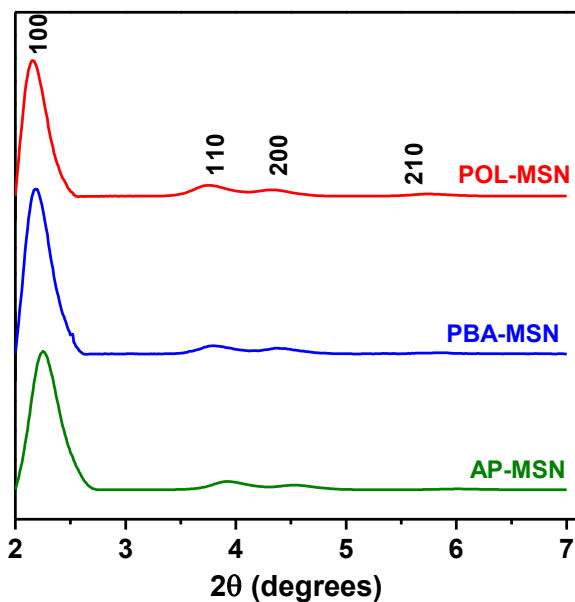


**Fig. S3.** Powder X-ray diffraction patterns of AP-MSN, PBA-MSN and POL-MSN

MSNs and POL-MSNs were recorded. The characteristic intense reflection peak (100) at low angle region between 2.0 to 2.4 ( $2\theta$ ) and another two to three low intense reflection peaks (110, 200, 210) at 3 to 6.5 ( $2\theta$ )<sup>S3</sup> confirmed (Fig. S3) the existence of 2D hexagonal arrays of unidimensional channels of MCM-41 in all the samples. Further, it proved that chemical modification of the surface of the MSN has no effect on the pore morphology of the MCM-41.

#### 4.2 Nitrogen adsorption-desorption isotherms

Surface area analysis of MCM-41, AP-MSN and POL-MSN were carried out using N<sub>2</sub> adsorption-desorption isotherms and the surface areas were calculated using the Brunaur-Emmett-Teller (BET) method. The characteristic “type IV” adsorption-desorption isotherms with H1-type hysteresis<sup>S4</sup> were observed (Fig. S4) for MCM-41 MSN before and after the surface functionalisation. BET Calculations reveal that the specific surface area of MCM-41 is 1240 m<sup>2</sup>g<sup>-1</sup>, while the surface area is 735 m<sup>2</sup>g<sup>-1</sup> for the surface-modified end-capped POL-MSN. The reduction of BET surface area of the final product in comparison to the starting materials indicates that surface functionalisation of MCM-41 has been achieved.

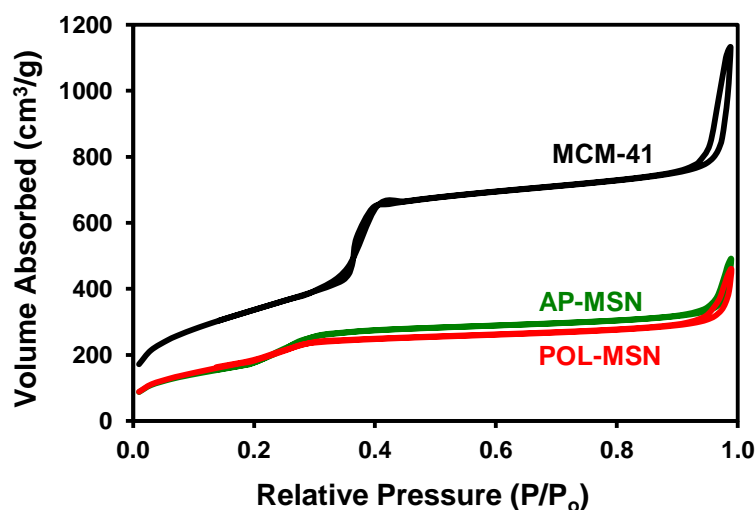


**Fig. S4.** Nitrogen adsorption-desorption isotherms of MCM-41, AP-MSN and POL-MSN

### 4.3 Transmission electron micrographs

Transmission electron microscopy (TEM) images were recorded in order to characterise the mesoporosity of MCM-41 before and after the surface modification.<sup>S3</sup> TEM Images demonstrated (Fig. S5a–c) that the porosity of MCM-41 remained intact after the surface modification, in support of the bulk results observed with powder diffraction. Further, TEM images of POL-MSN indicated (Fig. S5c) that the polymer-capping procedure explained in *Section 3.3* avoids the agglomeration of surface-functionalised MSN into larger aggregates. In agreement with the literature,<sup>S5</sup> a monolayer of polymer on the outer surface of the POL-MSN is hardly distinguishable in the TEM images (Fig. S5d).

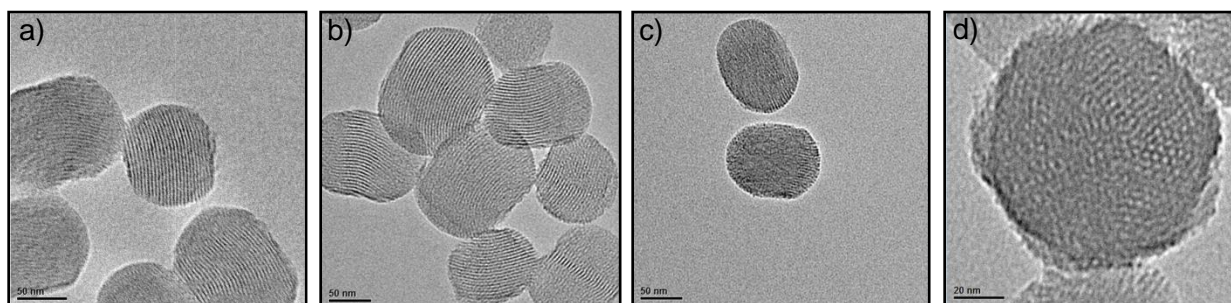


**Fig. S5.** Transmission electron micrographs of a) MCM-41, b) PBA-MSN, c) POL-MSN and d) POL-MSN.

### 4.4 Surface charge

$\zeta$  Potential values provide important information of alteration of the surface charge as a result of surface functionalisation. A suspension of the functionalised MSN in deionised H<sub>2</sub>O was used for the surface charge experiments.

Negative potential (−22.4 mV) of MCM-41 indicates the presence of negatively charged silanol groups on the silica surface. After modification of MCM-41 with amino functional groups, surface charge changed into a positive value (+14.6 mV) representing protonated cationic amino groups on the outer surface of the MSNs. Moreover, PBA-MSNs yield a negative surface charge

value (−1.79 eV), indicating the presence of negatively charged hydroxyl groups on the outer surface. Additionally, the positive  $\zeta$  potential of the POL-MSN demonstrates that the outer poly( $\beta$ -amino ester) layer has a slight positive charge at neutral pH. It is attributed to the protonation of amino group on the polymer backbone in the aqueous medium. Alteration of the sign of the  $\zeta$  potential values from MCM-41, AP-MSN, PBA-MSN to POL-MSN are in an agreement with the surface-functionalised MSN species.<sup>S1</sup>

| Material | $\zeta$ Potential (mV) |
|----------|------------------------|
| MCM-41   | −22.4                  |
| AP-MSN   | +14.6                  |
| PBA-MSN  | −1.79                  |
| POL-MSN  | +4.84                  |

**Table S1.**  $\zeta$  Potential values of MCM-41, AP-MSN, PBA-MSN and POL-MSN

#### **4.5 X-Ray photoelectron spectroscopy (XPS)**

X-Ray photoelectron spectroscopy (XPS) was used to evaluate the monolayer formation on the MSN.<sup>S6</sup> Appearance of F(1s) and B(1s) peaks in XPS traces of both PBA-MSN and POL-MSN at 686 and 191 eV, respectively, confirm (Fig. S6) the existence of covalently attached 4-fluorophenylboronic acid on the surface of the MSN which is clearly absent in AP-MSN. Furthermore, an increase of ratio between the area under the peak of C(1s) : Si(2s) from AP-MSN, PBA-MSN to POL-MSN indicates the growth of organic portion over the silica portion on the MSN surface. Furthermore, it confirms the presence of covalently attached organic molecules on the surface of the MSN.

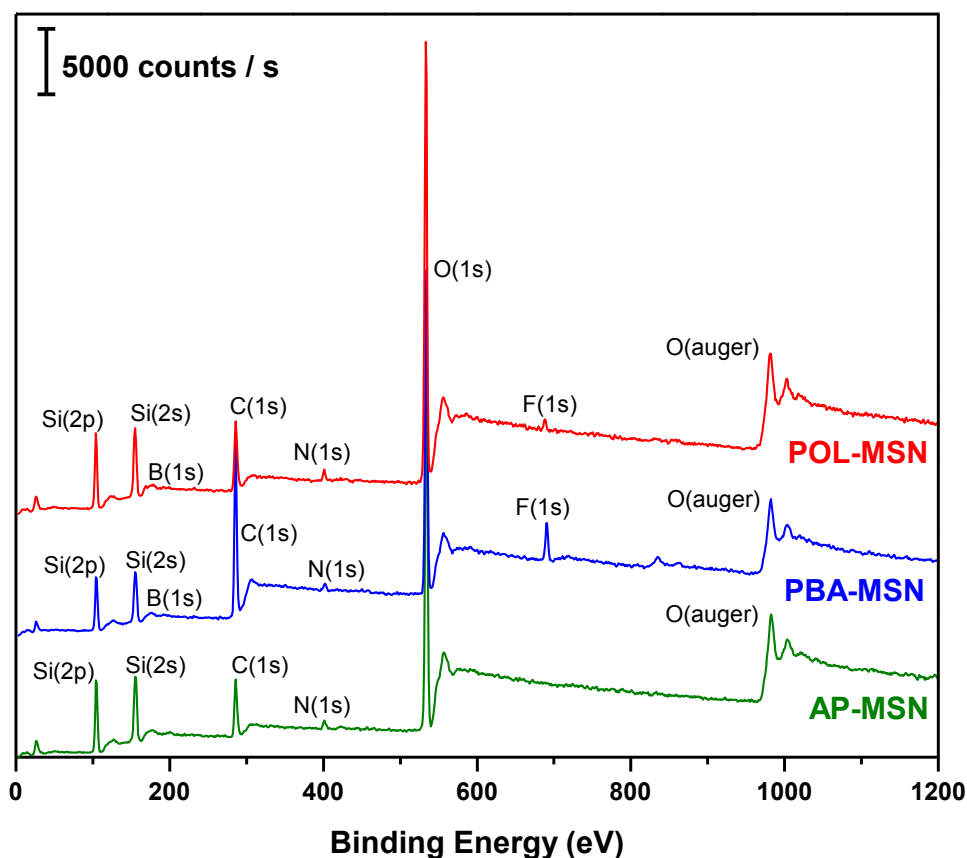


**Fig. S6.** XPS scans of AP-MSN, PBA-MSN and POL-MSN

#### 4.6 FT-IR spectroscopy

The surface functionalisation of MSN was also confirmed by FT-IR spectroscopy. All the samples show characteristic FT-IR peaks of the silica framework, corresponding to the asymmetric vibrations of Si–O and Si–OH at 1150 and 950  $\text{cm}^{-1}$  respectively. The symmetric vibration of Si–O appears (Fig. S7) at 800  $\text{cm}^{-1}$ . In surface modified MSN, a considerably large portion of the mass consists of silica, in which an organic portion is fairly insignificant (less than 5% by mass). Therefore, peaks derived from the organic portion are obscure in the IR spectrum. Very small bands around 2850–3000  $\text{cm}^{-1}$  and 1550–1640  $\text{cm}^{-1}$  regions, however, correspond to the C–H stretching and N–H bending, respectively.

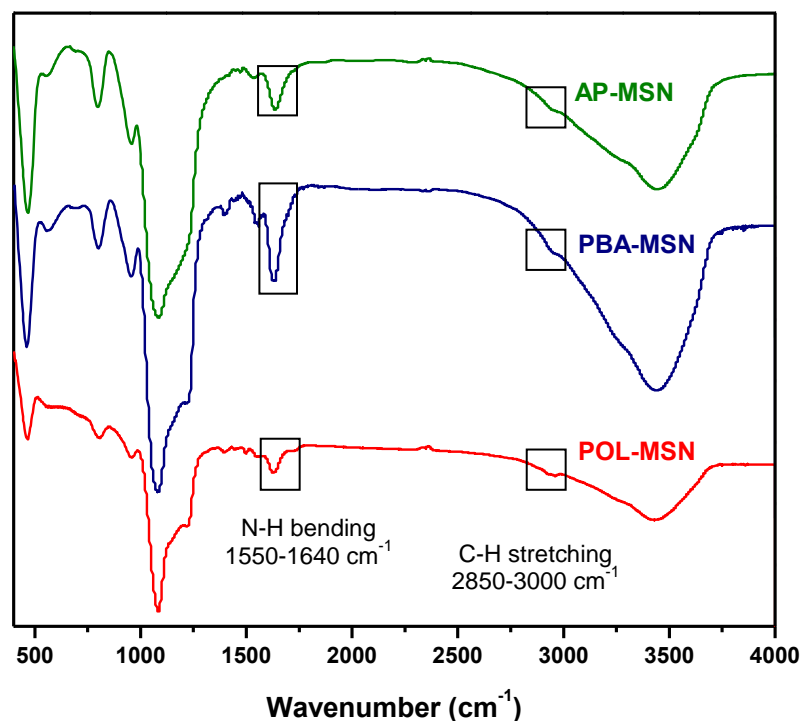


**Fig. S7.** FT-IR spectra of AP-MSN, PBA-MSN and POL-MSN

#### **4.7 Time-of-flight secondary ion mass spectrometry**

To evaluate the elemental composition of surface modified MSN time-of-flight secondary ion mass spectrometry (ToF SIMS) was performed<sup>S6</sup> on AP-MSN, PBA-MSN and POL-MSN. The mass fragments at 10 and 11 amu in ToF-SIMS spectra recorded (Fig. S8a-c) in positive-ion mode confirmed the presence of boron in PBA-MSN and POL-MSN samples which is clearly absent in the AP-MSN sample. Negative-ion ToF-SIMS data proved (Fig. S9a-c) the existence of fluorine as evidenced by the mass fragments at 19 amu which does not exist in AP-MSN.

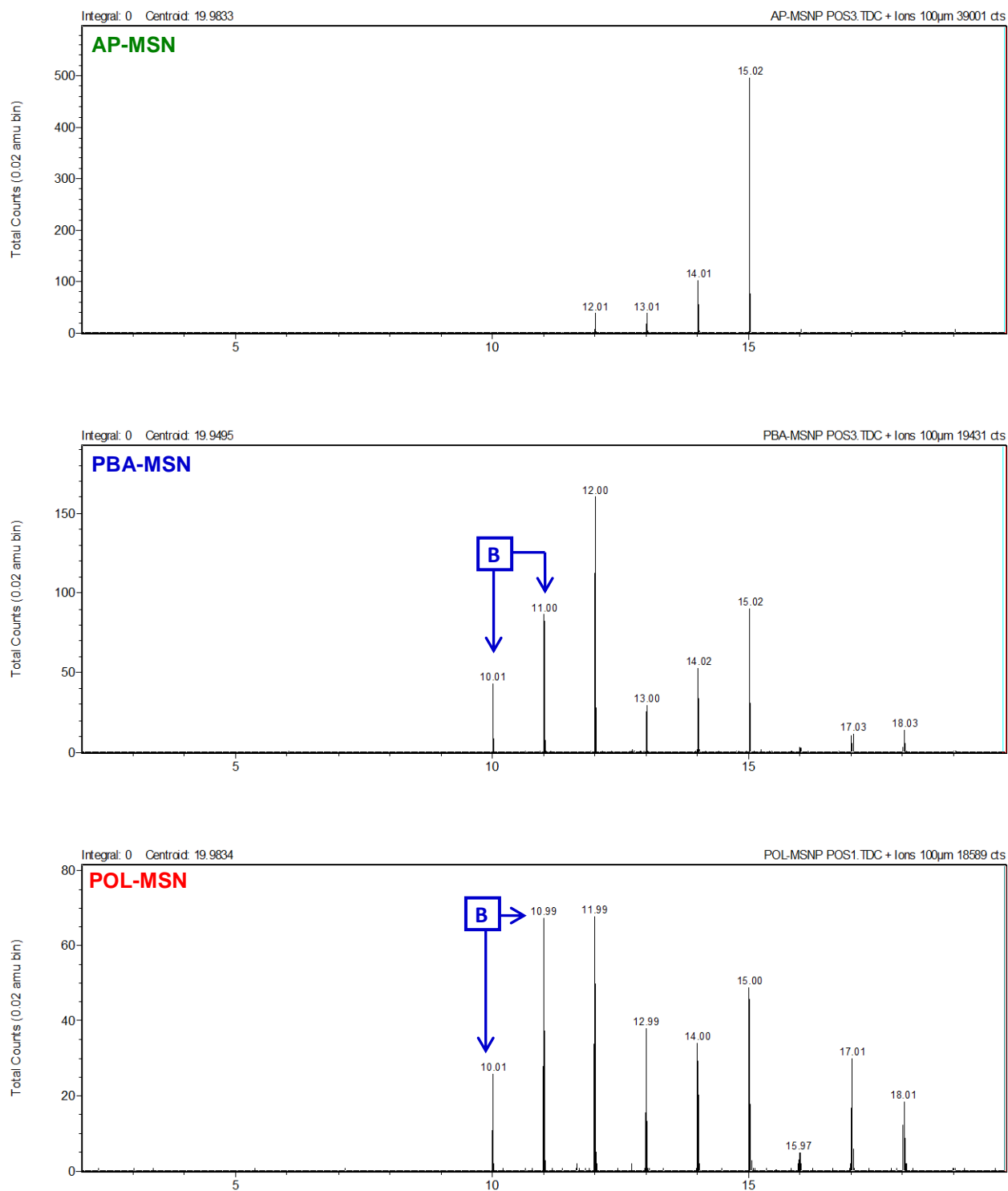


**Fig. S8.** Positive-ion ToF-SIMS spectra confirming the presence of boron in the PBA-MSN and POL-MSN which is absent in the AP-MSN

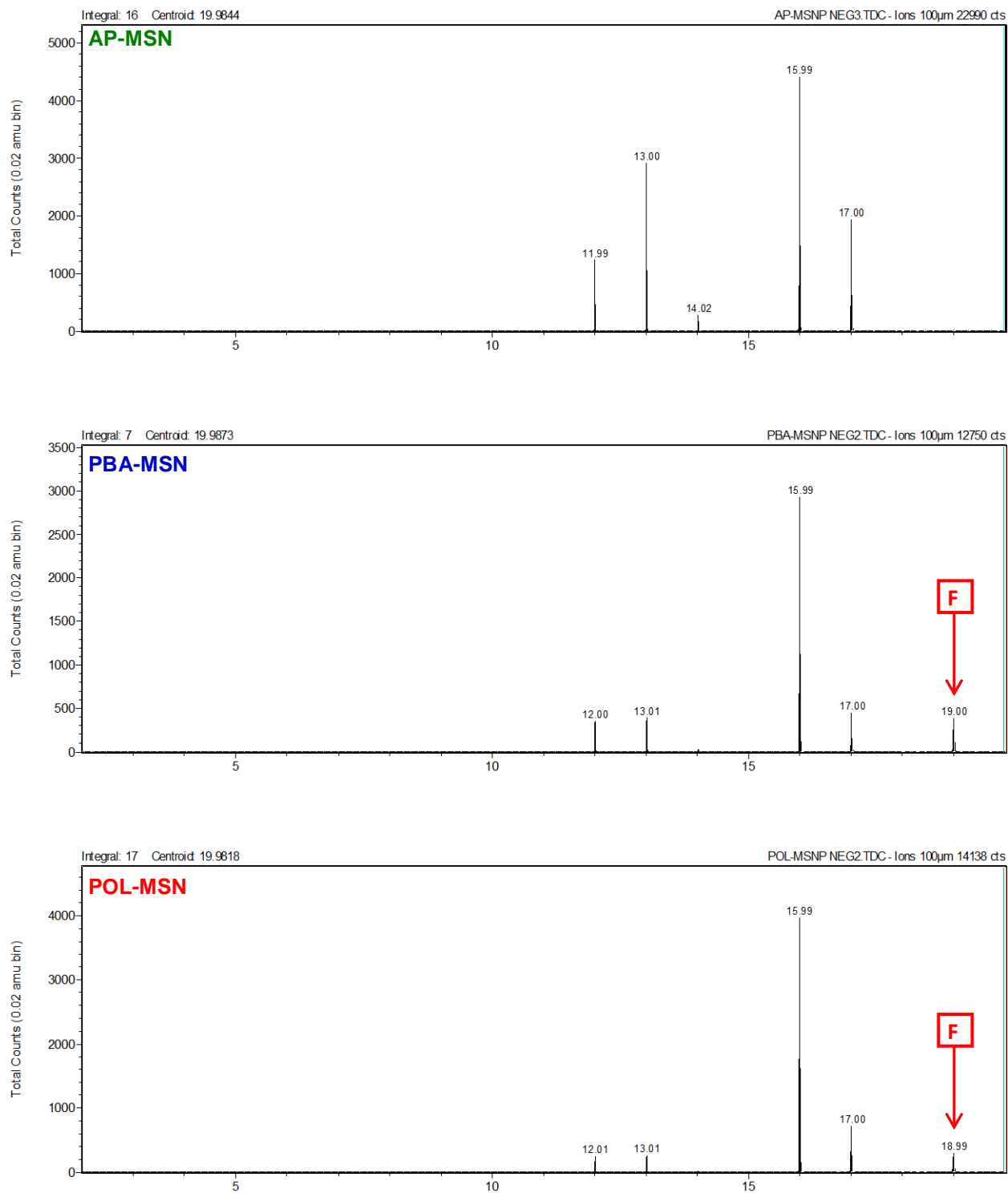
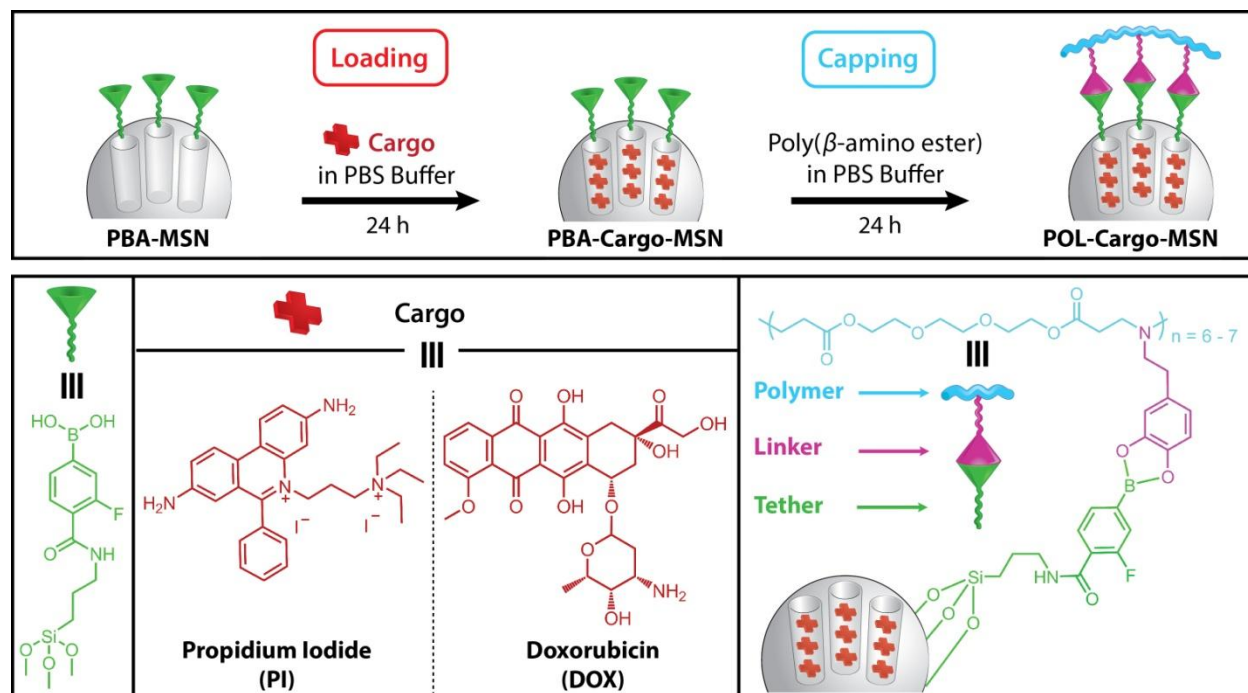


**Fig. S9.** Negative-ion ToF-SIMS spectra confirming the presence of fluorine in the PBA-MSN and POL-MSN which is absent in the AP-MSN

## 5. Cargo Loading and Capping



**Scheme S6.** Schematic representation of cargo loading and polymer capping

### 5.1 Propidium iodide loading and capping

PBA-MSNs (40 mg) were suspended in a propidium iodide (PI) solution (8 mL at a concentration of  $4 \text{ mg ml}^{-1}$ ) of pH 7.4 PBS buffer and stirred at room temperature for 24 h. An aqueous solution of the capping agent **POL** (80 mg) was added into the above suspension. The resulting mixture was stirred for another 24 h. This product was isolated by centrifugation and washed with copious amounts of  $\text{H}_2\text{O}$  and then dried under vacuum to obtain POL-PI-MSNs (43 mg).

### 5.2 Doxorubicin loading and capping

Doxorubicin (DOX) was loaded (8 mL at a concentration of  $1 \text{ mg ml}^{-1}$ ) into PBA-MSNs (40 mg) and capped with poly( $\beta$ -amino ester) by using the same procedure outlined in **Section 5.1** to obtain POL-DOX-MSNs (42 mg).

## 6. Cargo Release Studies in Solution

The pH and esterase enzyme responsive release of the cargo experiments were carried out using POL-PI-MSNs (3.5 mg) or POL-DOX-MSNs (1.0 mg). The sample was placed at the corner of quartz cuvette and pH 7.4 PBS buffer (2.50 mL) was added. The resulting mixture was stirred slowly to inhibit particle re-suspension, while increasing the rate of cargo release diffusion. The pH-triggered cargo release was achieved by adjusting the pH to the desired value with 1M HCl solution while esterase triggered release was achieved by adding a solution of porcine liver esterase (1 mg, 50 u/mg) in pH 7.4 PBS buffer (500  $\mu$ L). An excitation beam of 535 and 480 nm for PI and DOX, respectively was directed into the solution to excite the fluorescent emissions of the released cargo molecules. The fluorescence spectra (Fig. S10) were collected at every 10 min over the course of 2 h. Thereafter, fluorescence spectra were collected at every 30 min. Release profiles were obtained (Fig. 3) by plotting the time versus cargo emission at emission maxima.

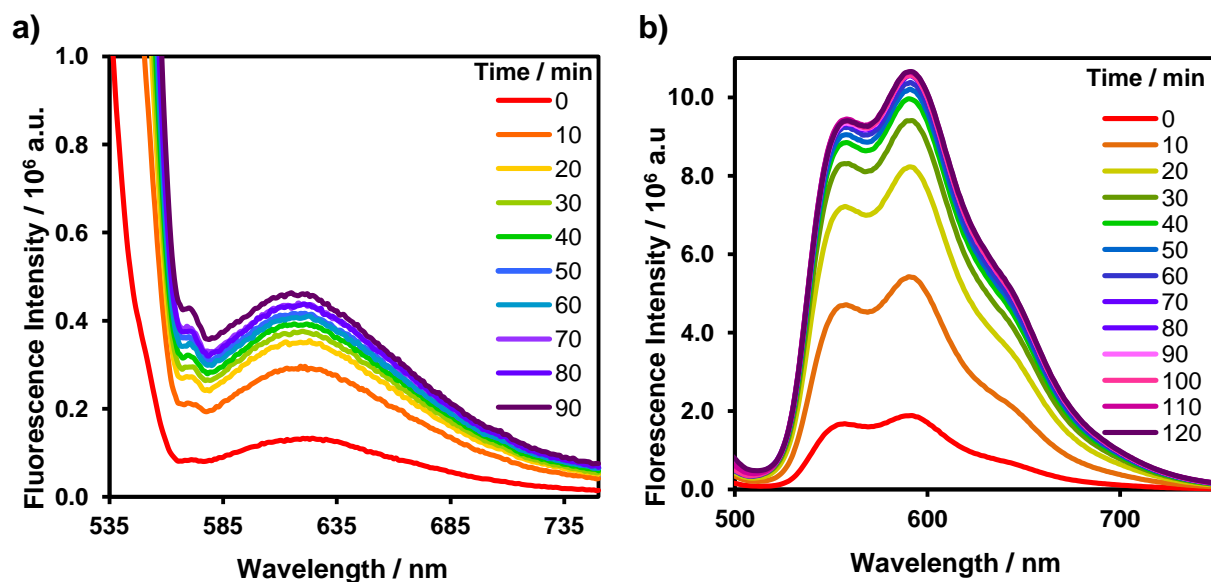


**Fig. S10.** Representative fluorescence spectra of a) PI and b) DOX with time, after adjusting the pH of the solution to 4.0

## 7. Cargo Release and Uptake Efficiencies and Capacities

The uptake and release capacities and efficiencies of PBA-MSNs loaded with the PI dye and the DOX anti-cancer therapeutic agent were investigated. The amount of cargo loaded inside the PBA-MSNs pores was calculated by subtracting the mass of the cargo remaining in the supernatant from the total mass of the cargo in the initial solution. The amount of cargo remained in the supernatant after the drug loading were calculated using a calibration curve of the corresponding cargo. The cargo uptake efficiency and capacity were calculated using the Equation 1 and 2, respectively.

$$\text{Uptake Efficiency (\%)} = \frac{\text{Mass of Cargo in MSNs}}{\text{Initial Mass of Cargo}} \quad (1)$$

$$\text{Uptake Capacity (\%)} = \frac{\text{Mass of Cargo in MSNs}}{\text{Mass of Cargo Loaded MSNs}} \quad (2)$$

pH or enzyme triggered mass of cargo release was calculated when the release profiles reach the plateau. The cargo release efficiency and capacity were calculated using the Equations 3 and 4, respectively.

$$\text{Release Efficiency (\%)} = \frac{\text{Mass of Cargo Released}}{\text{Total Mass of Cargo Uptake}} \quad (3)$$

$$\text{Release Capacity (\%)} = \frac{\text{Mass of Cargo Released}}{\text{Mass of Cargo Loaded MSNs}} \quad (4)$$

Uptake capacities and efficiencies of PI and DOX are given in the table S2.

**Table S2.** Uptake efficiencies and capacities of PI and DOX in PBS buffer at pH 7.4

| Cargo            | Uptake Efficiency % | Uptake Capacity % |
|------------------|---------------------|-------------------|
| Propidium Iodide | 73                  | 5.4               |
| Doxorubicin      | 68                  | 4.8               |

**Table S3.** Uptake / release efficiencies and capacities of PI and DOX in the presence of acid or esterase stimuli

| Stimuli   | PI                   |                    | DOX                  |                    |
|---|----------------------|--------------------|----------------------|--------------------|
|   | Release Efficiency % | Release Capacity % | Release Efficiency % | Release Capacity % |
| pH 7.4  | 17                   | 0.7                | 25                   | 0.3                |
| pH 6.0  | 42                   | 1.6                | 58                   | 1.3                |
| pH 5.0  | 53                   | 1.8                | 78                   | 2.2                |
| pH 4.0  | 83                   | 2.6                | 85                   | 2.4                |
| Esterase 1 mg, 50 u mg <sup>-1</sup><br>at pH 7.4 | 71                   | 2.4                | 77                   | 2.1                |

## 8. Cellular Imaging

Cellular uptake of the POL-PI-MSN and PI loaded, polymer-capped, fluorescein isothiocyanate (FITC) modified MSNs (POL-PI-FITC-MSNs) were investigated in MDA-MB-231 human breast cancer cells using fluorescence microscopy. Specifically, MDA-MB-231 cells were treated with POL-PI-MSN (50 µg/ml) or POL-PI-FITC (50 µg/ml) for 48 h. Cells were washed with PBS, fixed with 10% formalin, washed twice and stained with 4',6-diamino-2-phenylindole (DAPI). Images were taken using a Nikon Eclipse Ti-U fluorescence microscope. The fluorescent dye, (DAPI) was used to visualize the cell nuclei (Fig. S11a and e), and images with the blue emission were recorded after exciting at 405 nm. Upon internalisation of POL-PI-MSN and releasing the cargo, PI stained cell nuclei were observed (Fig. S11b) as red emissions, after exciting at 488 nm. The overlapped image of Fig. S11a and b shown in Fig. S11d confirms that the PI released from the hybrid nanocarriers stained the nuclei. In a manner similar to POL-PI-MSNs, POL-PI-FITC-MSNs releases PI into the cellular environment and stained the nuclei (Fig. S11f).

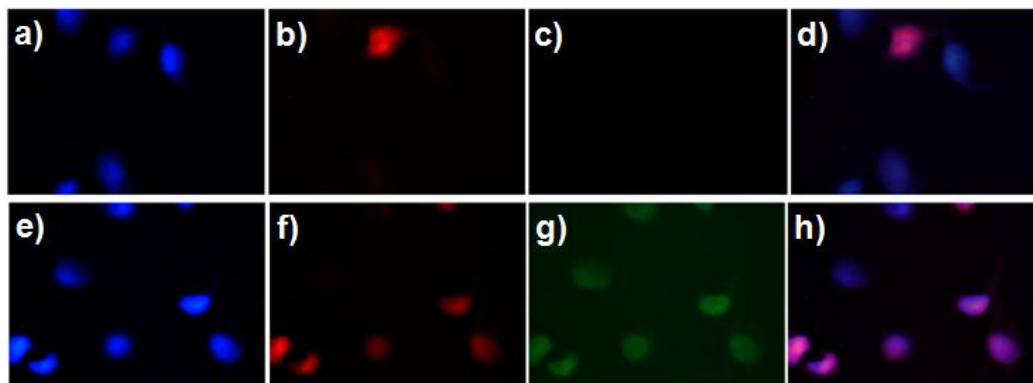


**Fig. S11.** Fluorescence microscopy images of MDA-MB-231 human breast cancer cells incubated with POL-PI-MSNs (top row, a–d) and POL-PI-FITC-MSNs (bottom row, e–h); The images of first (a,e), second (b,f), third (c,g) and fourth (d,h) columns show cellular staining of DAPI (in blue,  $\lambda_{\text{ex}} = 405$  nm,  $\lambda_{\text{em}} = 440\text{--}470$  nm), PI (in red,  $\lambda_{\text{ex}} = 525$  nm,  $\lambda_{\text{em}} = 550\text{--}570$  nm), FITC (in green,  $\lambda_{\text{ex}} = 488$  nm,  $\lambda_{\text{em}} = 500\text{--}530$  nm) and the overlay of DAPI and PI (in purple), respectively.

## 9. In-Vitro Cytotoxicity

Human MDA-MB-231 breast cancer cells were treated with vehicle (PBS pH 7.4), PBA-MSNs, POL-MSNs, POL-DOX-MSNs (all 64  $\mu\text{g}/\text{ml}$ ) and DOX (2  $\mu\text{g}/\text{ml}$ ) for 48 h, and the cells were then allowed to recover for 48 h in normal growth media. Surviving cells were stained with crystal violet as described.<sup>S7</sup> Images were captured and the % cell confluence was determined using NIH ImageJ software. Two experiments were performed, each in triplicate. The data are presented in Fig. 4.

## 10. References

**S1** Y. Zhao, B. G. Trewyn, I. I. Slowing and V. S.-Y. Lin, *J. Am. Chem. Soc.*, 2009, **131**, 8398–8400.

**S2** D. G. Anderson, A. Akinc, N. Hossain and R. Langer, *Mol. Ther.*, 2005, **11**, 426–434.

**S3** C. T. Kresge, M. E. Leonowicz, W. J. Roth, J. C. Vartuli and J. S. Beck, *Nature*, 1992, **359**, 710–712.

- S4** T. J. Barton, L. M. Bull, W. G. Klemperer, D. A. Loy, B. McEnaney, M. Misono, P. A. Monson, G. Pez, G. W. Scherer, J. C. Vartuli and O. M. Yaghi, *Chem. Mater.*, 1999, **11**, 2633–2656.
- S5** N. Singh, A. Karambelkar, L. Gu, K. Lin, J. S. Miller, C. S. Chen, M. J. Sailor and S. N. Bhatia, *J. Am. Chem. Soc.*, 2011, **133**, 19582–19585.
- S6** M. W. Ambrogio, M. Frasconi, Y. D. Yilmaz and X. Chen, *Langmuir*, 2013, **29**, 15386–15393.
- S7** M. Lu, A. Strohecker, F. Chen, T. Kwan, J. Bosman, V. C. Jordan and V. L. Cryns, *Clin. Cancer Res.*, 2008, **14**, 3168–3176.